

Effects of Si addition on mechanical properties of copper severely deformed by accumulative roll-bonding

Takahiro Kunimine · Toshiyuki Fujii ·
Susumu Onaka · Nobuhiro Tsuji · Masaharu Kato

Received: 30 August 2010/Accepted: 30 December 2010/Published online: 15 January 2011
© Springer Science+Business Media, LLC 2011

Abstract Effects of Si addition on mechanical properties of severely deformed copper by accumulative roll-bonding (ARB) have been investigated. Tensile tests and strain-rate jump tests have been carried out at room temperature. For annealed coarse-grained polycrystals, the difference in yield stress $\sigma_{0.2}$ between pure copper and a Cu–1.64at.%Si alloy was only about 15 MPa while the difference became 170 MPa after the ARB process by six cycles. The strain-rate sensitivity m of pure copper increased with increasing the number N of the ARB cycles for $N \geq 5$. However, the increase in m becomes less significant for Cu–Si alloys. These findings have been discussed in terms of thermally activated dislocation processes.

Introduction

Ultrafine grains (UFGs) in the range of 100 nm–1 μm are often formed by severe plastic deformation (SPD) [1, 2]. Enhanced mechanical properties and higher strain-rate

dependence of flow stress σ for UFG FCC metals compared with those for coarse-grained (CG) counterparts have been the subjects of extensive studies [3–11]. However, little is known about the effects of solute atoms on mechanical properties prepared by SPD. In particular, the effects of solute addition on the strain-rate dependence of the flow stress σ have not been studied in detail for UFG materials. The purpose of this article is to investigate the effects of Si addition on mechanical properties of severely deformed copper by the accumulative roll-bonding (ARB) [12, 13].

Experimental procedure

Copper and Cu–Si solid-solution alloys, i.e., pure copper of 99.99% purity (4NCu), a Cu–0.41at.%Si alloy (Cu0.4Si) and a Cu–1.64at.%Si alloy (Cu1.6Si) were chosen for experiments. Annealed and CG polycrystalline sheets were used as primary materials. The ARB processes giving an equivalent strain of 0.8 per one cycle [13] were performed at room temperature (RT). The numbers N of the ARB cycles were up to $N = 8$ (4NCu), $N = 10$ (Cu0.4Si), and $N = 6$ (Cu1.6Si). Because of the initiation of large cracks at the edges of specimens, it was impossible to continue ARB processes after the above cycles. Tensile specimens with 10-mm gauge length, 3-mm gauge width, and 1-mm gauge thickness were cut from the ARB processed specimens with an electro discharge machine. For comparison, specimens cut from the annealed CG polycrystalline sheets before ARB were also prepared. Tensile tests were carried out at RT with an Instron-type testing machine at a base strain rate $\dot{\varepsilon}$ of $8.3 \times 10^{-5} \text{ s}^{-1}$. Strain-rate jump tests were performed to evaluate the strain-rate sensitivity m defined by

T. Kunimine (✉) · S. Onaka · M. Kato
Department of Materials Science and Engineering, Tokyo Institute of Technology, 4259 Nagatsuta-cho, Midori-ku, Yokohama 226-8502, Japan
e-mail: kumiminet9@gmail.com

T. Fujii
Department of Innovative and Engineered Materials, Tokyo Institute of Technology, 4259 Nagatsuta-cho, Midori-ku, Yokohama 226-8502, Japan

N. Tsuji
Department of Materials Science and Engineering, Graduate School of Engineering, Kyoto University, Yoshida Honmachi, Sakyo-ku, Kyoto 606-8501, Japan

$$m = \frac{\partial \ln \sigma}{\partial \ln \dot{\varepsilon}} = \frac{1}{\sigma} \frac{\partial \sigma}{\partial \ln \dot{\varepsilon}}. \quad (1)$$

When a strain-rate jump from $\dot{\varepsilon}_1 = 8.3 \times 10^{-5} \text{ s}^{-1}$ to $\dot{\varepsilon}_2 = 8.3 \times 10^{-4} \text{ s}^{-1}$ causes the change in the flow stress from σ_1 to σ_2 , m can be written as

$$m = \frac{(\sigma_2 - \sigma_1)}{[(\sigma_1 + \sigma_2)/2] \ln(\dot{\varepsilon}_2/\dot{\varepsilon}_1)}. \quad (2)$$

The microstructural characterization of the ARB processed specimens was carried out by electron backscattering diffraction pattern (EBSP) measurements with a field emission type scanning electron microscope (FE-SEM). The microstructures of the ARB processed specimens were observed from the transverse direction (TD) of the sheet. Boundaries with a misorientation angle θ smaller than 2° were neglected.

Results

Microstructure of ARB processed copper and Cu–Si alloy

Figure 1 shows grain-boundary maps obtained by the EBSP measurements of the ARB processed (a) 4NCu for $N = 7$ and (b) Cu0.4Si for $N = 6$. Green and red lines indicate high- ($\theta \geq 15^\circ$) and low-angle ($2^\circ \leq \theta < 15^\circ$) boundaries, respectively. In Fig. 1, ultrafine lamellar boundary

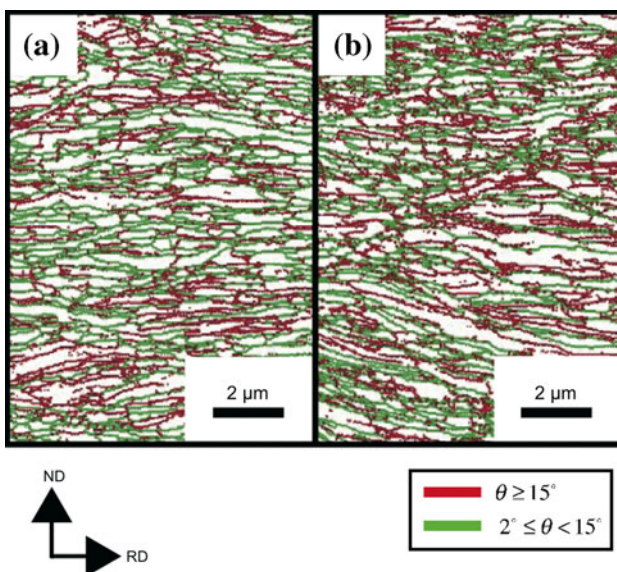


Fig. 1 Boundary maps of ARB processed **a** 4NCu with $N = 7$ and **b** Cu0.4Si with $N = 6$ obtained by EBSP measurement. In this boundary maps, red lines indicate the misorientation of $2^\circ \leq \theta < 15^\circ$, while green lines indicate the one of $\theta \geq 15^\circ$. RD and ND are the rolling and normal directions of the ARB process, respectively. For interpretation of the references to colour in this figure legend, the reader is referred to the web version of this article

structures formed by high-angle boundaries were found in both 4NCu and Cu0.4Si. The morphology of the microstructure observed in the ARB processed Cu0.4Si with $N = 6$ was quite similar to that of the ARB processed 4NCu with $N = 7$. The microstructural parameters obtained from the EBSP measurements were summarized in Table 1, where d_{HAGB} is the mean spacing of the high-angle boundaries along the normal direction (ND) and f_{HAGB} the fraction of high-angle boundaries. As shown in Table 1, d_{HAGB} and f_{HAGB} for the ARB processed 4NCu and Cu0.4Si were almost the same.

Effects of Si addition on the stress–strain curves

Figure 2 shows the true stress–true strain (σ – ε) curves at RT for the ARB processed specimens with $N = 6$ of 4NCu, Cu0.4Si, and Cu1.6Si. These results were obtained by the tensile tests under a base strain rate $\dot{\varepsilon}$ of $8.3 \times 10^{-5} \text{ s}^{-1}$. The true stress–true strain (σ – ε) curves were obtained from the nominal stress–nominal strain curves by assuming uniform deformation. Remarkable changes in ductility and strain-hardening rate with Si addition have not been observed in this study. The steps on the σ – ε curves are the changes $\Delta\sigma$ in the flow stress σ caused by the strain-rate jump tests between $8.3 \times 10^{-5} \text{ s}^{-1}$ and $8.3 \times 10^{-4} \text{ s}^{-1}$. The changes $\Delta\sigma$ associated with the strain-rate jump are

Table 1 Microstructural parameters obtained from the EBSP measurements of the ARB processed specimens

Specimens	d_{HAGB} (nm)	f_{HAGB} (%)
4NCu for $N = 7$	370	56
Cu0.4Si for $N = 6$	320	54

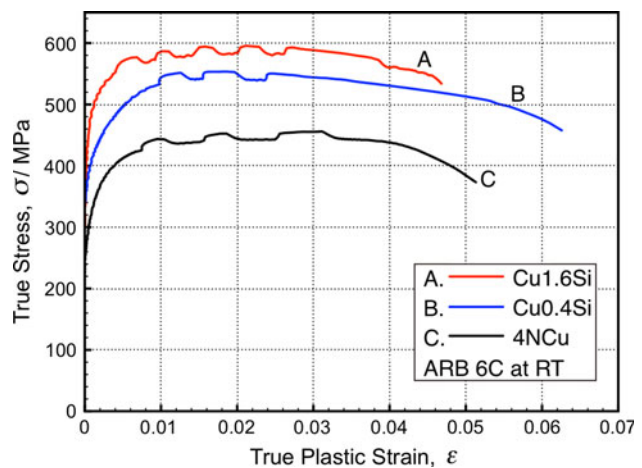


Fig. 2 The true stress–true strain (σ – ε) curves at RT for the ARB processed specimens with $N = 6$ of 4NCu and Cu–Si alloys. The steps on the σ – ε curves are the changes in the flow stress σ caused by the strain-rate jump tests between $8.3 \times 10^{-5} \text{ s}^{-1}$ and $8.3 \times 10^{-4} \text{ s}^{-1}$

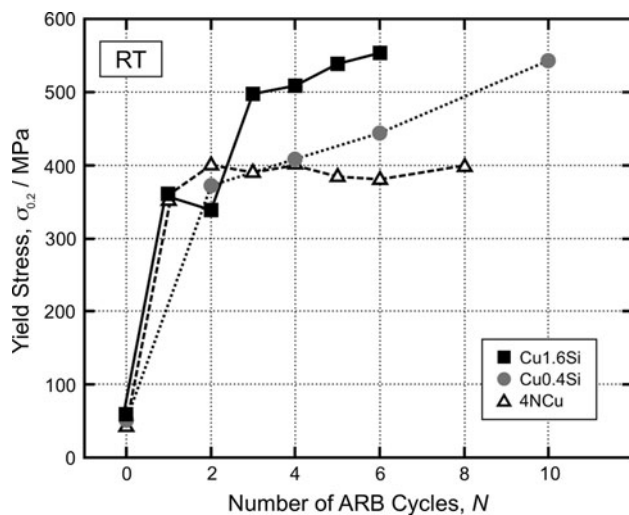


Fig. 3 The relationships between the number N of ARB cycles and the yield stress $\sigma_{0.2}$ tensile tested at RT under a strain rate $\dot{\varepsilon}$ of $8.3 \times 10^{-5} \text{ s}^{-1}$ for the specimens of 4NCu and Cu–Si alloys

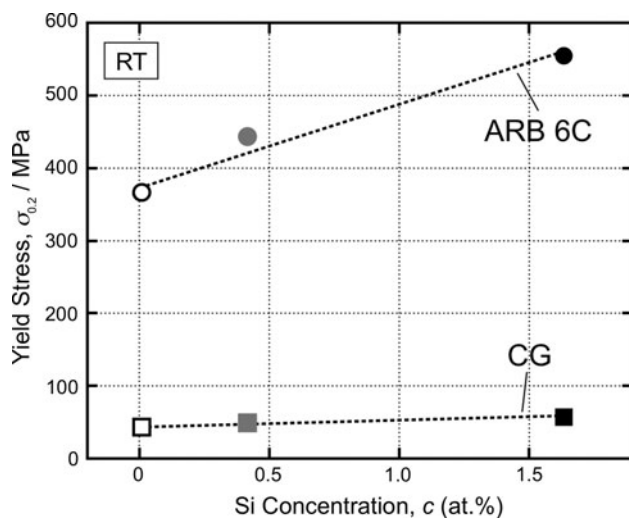


Fig. 4 Effects of the Si concentration c on the yield stress $\sigma_{0.2}$ of the annealed CG polycrystalline specimens and ARB processed specimens with $N = 6$ tensile tested at RT under a strain rate $\dot{\varepsilon}$ of $8.3 \times 10^{-5} \text{ s}^{-1}$

about 14 MPa for 4NCu, 12 MPa for Cu0.4Si, and 14 MPa for Cu1.6Si at a true plastic strain of $\varepsilon \approx 0.01$.

Figure 3 shows the variation of the yield stress $\sigma_{0.2}$ as a function of the number N of ARB cycles. The yield stress of 4NCu increases with increasing N to $N = 2$ and stays at about 400 MPa for N larger than 2, in good agreement with the previous report by Takata et al. [14]. On the other hand, the yield stresses $\sigma_{0.2}$ of Cu0.4Si and Cu1.6Si continue to increase with increasing N . These results indicate that the Si addition has large effects on the increase in the yield stresses $\sigma_{0.2}$ of the ARB processed copper.

Figure 4 shows the effects of the Si concentration c on the yield stress $\sigma_{0.2}$ of the annealed CG specimens and the

ARB processed specimens with $N = 6$. For the CG specimens, the difference $\Delta\sigma_{0.2}$ in $\sigma_{0.2}$ between 4NCu and Cu1.6Si is about 15 MPa. This amount of $\Delta\sigma_{0.2}$ can be understood reasonably as a result of the usual solid-solution strengthening caused by the interaction between dislocations and solute atoms [15]. However, the ARB process significantly increases both $\sigma_{0.2}$ and $\Delta\sigma_{0.2}$ of the Cu–Si alloys and $\Delta\sigma_{0.2}$ becomes as large as 170 MPa. This large increase in $\Delta\sigma_{0.2}$ cannot be understood as a result of the usual solid-solution strengthening. As shown in Fig. 1 and Table 1, the Si addition does not significantly change the mean spacing of the high-angle boundaries of the ARB processed specimens. Therefore, neither the solid-solution strengthening nor the spacing of the high-angle boundaries can explain the large difference in $\Delta\sigma_{0.2}$ of the ARB processed specimens with and without the Si addition.

Effects of Si addition on the strain-rate sensitivity

Figure 5 shows the relationships between true stress σ and calculated strain-rate sensitivity m using Eq. 2. For CG 4NCu (open squares), m is nearly constant even when σ increases by strain hardening during tensile deformation. This result has been understood as the Cottrell–Stokes law [8, 11, 16–18]. The data points shown by open circles and triangles are the results of the ARB processed low-cycle (from $N = 1$ to 4) and high-cycle (from $N = 5$ to 8) specimens of 4NCu, respectively. As can be seen, the strain-rate sensitivity m of 4NCu increases with increasing the ARB cycles N from $m \approx 0.005$ (CG) to $m \approx 0.018$ ($N = 8$). The increase in the strain-rate dependence of flow stress is one of the characteristic features of FCC pure metals after SPD [3–11].

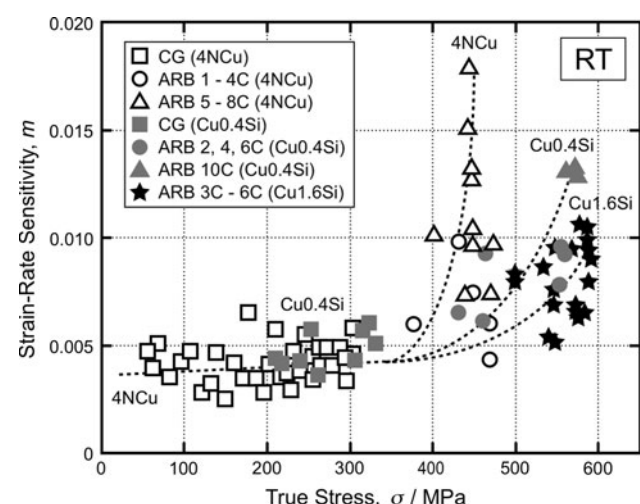


Fig. 5 The relationships between the true stress σ and the strain-rate sensitivity m at RT for the annealed CG polycrystalline specimens and ARB processed specimens of 4NCu and Cu–Si alloys

Effects of the Si addition on the strain-rate sensitivity m have also been investigated. The variation of m in CG Cu0.4Si (closed squares) is almost the same as that in CG 4NCu when σ is about 200–300 MPa as shown in Fig. 5. The data points shown by closed circles and triangles are the results of ARB processed Cu0.4Si. It is true that the ARB process increases m , but m is at most 0.013 even for the ARB processed specimen with $N = 10$ of Cu0.4Si, as compared to 0.018 for 4NCu. Similarly, m is at most 0.011 in the ARB processed Cu1.6Si. From the above experimental results, we conclude that the Si addition suppresses the increase of m with increasing N .

Discussion

Rate-controlling deformation mechanism and activation volume

A deformation mechanism map for FCC metals as a function of grain size has been given by Cheng et al. [19]. Although both grain-boundary and intragranular dislocation sources operate, intragranular deformation mechanisms are much more dominant in CG metals [19]. On the other hand, dislocation sources at grain boundaries become more dominant as grain size falls into UFG and nanocrystalline regimes [19]. Generation of dislocations at grain boundaries and their successive motion in UFG pure metals has been studied [20, 21].

Let us now consider the activation volume V^* , which is an effective parameter to examine the rate-controlling deformation mechanism. It is written as a function of m [11],

$$V^* = M \frac{kT}{m\sigma}, \quad (3)$$

where M is the Taylor factor of 3.06 for FCC metals, k the Boltzmann constant, and T the absolute temperature. In this study, V^* was evaluated from m in Fig. 5 using Eq. 3.

Figure 6 shows the activation volume V^* as a function of σ at RT for the ARB processed specimens used in this study. The vertical axis of Fig. 6 indicates V^* normalized by b^3 , where $b = 0.25$ nm is the magnitude of the Burgers vector for Cu. We can see that the data points of CG (open squares) and ARB processed 4NCu with $N = 1$ to 4 (open circles) lie on a single straight line with a slope of -1 , i.e., the upper broken line in the log–log plot in Fig. 6. This σ – V^* relationship is explained with the Taylor equation when the rate-controlling deformation mechanism is the cutting of forest dislocations by moving dislocations in the grain interior [11]. For the severely deformed 4NCu with $N = 5$ to 8 (open triangles), obvious deviation from the above straight line is found. This behavior has been

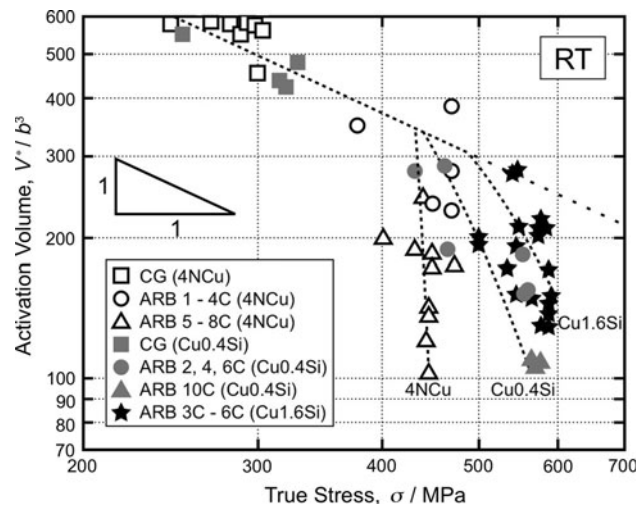


Fig. 6 The activation volume V^* as a function of the true stress σ at RT for the annealed CG polycrystalline specimens and the ARB processed specimens of 4NCu and Cu–Si alloys. The vertical axis indicates V^* normalized by b^3 , where $b = 0.25$ nm is the magnitude of the Burgers vector for Cu

explained by the transition of the rate-controlling deformation mechanism from that in the grain interior to that at grain boundaries [11, 20, 21].

Effects of Si addition on strength

In Fig. 6, we find that the data points of the CG Cu0.4Si (closed squares) are on the same broken line with the slope of -1 . The Si addition to CG specimens does not change the σ – V^* relationship. When the strengthening is explained by the Taylor equation, we have

$$\sigma = \alpha M \mu b \sqrt{\rho}, \quad (4)$$

where α is a constant (0.3–0.6), μ the shear modulus, b the magnitude of Burgers vector, and ρ the dislocation density in the grain interior. Gubicza et al. [22, 23] have reported that the addition of small amount of Mg significantly increases the strength of SPD Al by equal-channel angular pressing (ECAP). According to them, the addition of Mg suppresses the annihilation of dislocations in the Al matrix during SPD and increases the dislocation density ρ in the grain interior [23]. From the Taylor equation, one may think that the present strengthening by the Si addition is also due to the increase in ρ . One of the reasons of the increase in ρ is the decrease in the stacking fault energy (SFE). Effects of Si addition on SFE have been discussed in previous studies [24–26]. The values of SFE for Cu [27] and Cu–1.7at%Si alloy [26] have been reported as 45 and 35 mJ m⁻², respectively. The Si addition decreases SFE generally and may cause the increase in ρ . Then, the large increase in $\Delta\sigma_{0.2}$ from 15 to 170 MPa (Fig. 4) may well be reasonably explained if an appropriate increase in ρ is

assumed for UFG Si-containing alloys. However, we believe this interpretation leaves room for improvement to understand the present results.

If the strengthening by the Si addition is explained by Eq. 4, we can expect that the results of the σ – V^* relationships lie on the line with a slope of -1 [11]. However, SPD changes this situation. The data points shown by closed symbols in Fig. 6 are the results of the ARB processed specimens for Cu0.4Si with $N = 2$ to 6 (closed circles) and with $N = 10$ (closed triangles). These results of the ARB processed Cu–Si alloys deviate from the line depending on the degree of SPD. The same is true for the ARB processed Cu1.6Si from $N = 3$ to 6. The deviation is significant for the severely ARB processed alloys. This means that the large difference in $\Delta\sigma_{0.2}$ in Fig. 4 cannot be due solely to the effect of the increase in dislocation density by the Si addition. One important thing we notice from Fig. 6 is that the deviation from the straight line occurs less significantly at higher stresses as Si content becomes higher. To understand these results, only the consideration of the dislocation–dislocation interactions in the grain interior is not sufficient.

Effects of Si addition on rate-controlling deformation mechanism

Similar to the case of copper [11, 20, 21], the deviation of the σ – V^* relationship from the straight line with the slope of -1 in the UFG Cu–Si alloys may be explained by the transition of the rate-controlling deformation mechanism from that in the grain interior to that at grain boundaries. In pure copper with UFGs, emission and bow out of dislocations are considered to be the mechanism at grain boundaries [19–21]. From this point of view, the σ – V^* relationships for the Cu–Si alloys in Fig. 6 suggest that the Si addition causes the transition of the dominant mechanisms at higher σ . It is probable that the dislocation–dislocation interactions in grain interior and the dislocation reactions at grain boundaries coexist and which is more important depends on the Si content and the number of the ARB cycles.

As a reason of this effect of the Si addition, we can point out the suppression of dislocation reactions at grain boundaries by segregation of Si atoms. It is well known that marked grain-boundary segregation of solute atoms occurs in the UFG and nanocrystalline materials [28–31]. The segregated atoms can act as additional obstacles for grain-boundary dislocations to bow out into grain interiors, resulting in higher stresses necessary for the initiation of the dislocation bow out. Therefore, if the dislocation reactions at grain boundaries are suppressed by the Si segregation, it is natural that the transition to the grain-boundary mechanism is more retarded with increasing the

Si content. In fact, the required higher stresses caused by the retardation effect are not inconsistent with the observed much larger value of $\Delta\sigma_{0.2}$ in UFG alloys. Although further studies are needed, these interpretations reasonably explain the results of the σ – V^* relationships shown in Fig. 6.

Conclusions

Effects of Si addition on mechanical properties of severely deformed copper by ARB have been investigated at RT. The important findings of this study are:

- (1) For annealed coarse-grained polycrystals, the difference in yield stress $\sigma_{0.2}$ between pure copper and a Cu–1.64at.%Si alloy was only about 15 MPa while the difference in $\sigma_{0.2}$ became 170 MPa after the ARB process by six cycles.
- (2) The strain-rate sensitivity m of pure copper increased with increasing the number N of ARB cycles for $N \geq 5$. However, the increase in m becomes less significant for Cu–Si alloys.
- (3) The relationships between the activation volume V^* and the flow stress σ for both pure copper and Cu–Si alloys with coarse grains are explained by a single straight line with a slope of -1 in the log–log plot. Although the deviation from the straight line occurs for both the severely ARB processed pure Cu and Cu–Si alloys, it occurs at higher σ as Si content becomes higher.

Acknowledgements This research was supported by a Grant-in-Aid for Scientific Research on Innovative Areas “Bulk Nanostructured Metals” (22102006) from the Ministry of Education, Culture, Sports, Science and Technology (MEXT) of Japan. T. Kunimine is grateful for the support of the Global COE Program (Education and Research Center for Material Innovation) in Tokyo Institute of Technology, MEXT, Japan. The authors are grateful to Dr. Naoki Takata (Tokyo Institute of Technology, Japan) for performing the EBSP measurements.

References

1. Meyers MA, Mishra A, Benson DJ (2006) Prog Mater Sci 51:427
2. Azushima A, Kopp R, Korhonen A, Yang DY, Micari F, Lahoti GD, Groche P, Yanagimoto J, Tsuji N, Rosochowski A, Yanagida A (2008) CIRP Ann Manuf Technol 57:716
3. Wang YM, Ma E (2003) Appl Phys Lett 83:3165
4. Wei Q, Cheng S, Ramesh KT, Ma E (2004) Mater Sci Eng A 381:71
5. Dalla Torre FH, Pereloma EV, Davies CHJ (2004) Scr Mater 51:367
6. May J, Höppel HW, Göken M (2005) Scr Mater 53:189
7. Höppel HW, May J, Eisenlohr P, Göken M (2005) Z Metallkd 96:566

8. Dalla Torre FH, Pereloma EV, Davies CHJ (2006) *Acta Mater* 54:1135
9. Dalla Torre FH, Gazder AA, Pereloma EV, Davies CHJ (2007) *J Mater Sci* 42:1622. doi:[10.1007/s10853-006-1283-1](https://doi.org/10.1007/s10853-006-1283-1)
10. Wei Q (2007) *J Mater Sci* 42:1709. doi:[10.1007/s10853-006-0700-9](https://doi.org/10.1007/s10853-006-0700-9)
11. Kunimine T, Takata N, Tsuji N, Fujii T, Kato M, Onaka S (2009) *Mater Trans* 50:64
12. Tsuji N, Saito Y, Utsunomiya H, Tanigawa S (1999) *Scr Mater* 40:795
13. Tsuji N (2006) In: Altan BS, Miskioglu I, Purcek G, Mulyukov RR, Artan R (eds) Severe plastic deformation: towards bulk production of nanostructured materials. NOVA Science Publishers, New York
14. Takata N, Lee SH, Lim CY, Kim SS, Tsuji N (2007) *J Nanosci Nanotechnol* 7:3985
15. Wille T, Gieseke W, Schwink C (1987) *Acta Metall* 35:2679
16. Cottrell AH, Stokes RJ (1955) *Proc R Soc A* 233:17
17. Bochniak W (1993) *Acta Metall Mater* 41:3133
18. Bochniak W (1995) *Acta Metall Mater* 43:225
19. Cheng S, Spencer JA, Milligan WW (2003) *Acta Mater* 51:4505
20. Kato M, Fujii T, Onaka S (2008) *Mater Trans* 49:1278
21. Kato M (2009) *Mater Sci Eng A* 516:276
22. Gubicza J, Chinh NQ, Horita Z, Langdon TG (2004) *Mater Sci Eng A* 387–389:55
23. Gubicza J, Chinh NQ, Csanadi T, Langdon TG, Ungar T (2007) *Mater Sci Eng A* 462:86
24. Gallagher PCJ (1970) *Metall Trans* 1:2429
25. Nordstrom TV, Barrett CR (1969) *Acta Metall* 17:139
26. Carter CB, Ray ILF (1977) *Philos Mag* 35:189
27. Hirth JP, Lothe J (1982) Theory of dislocations. Wiley, New York
28. Nurislamova G, Sauvage X, Murashkin M, Islamgaliev R, Valiev R (2008) *Philos Mag Lett* 88:459
29. Valiev RZ, Enikeev NA, Murashkin MY, Kazykhanov VU, Sauvage X (2010) *Scr Mater* 58:949
30. Jang S, Purohit Y, Irving D, Padgett C, Brenner D, Scattergood RO (2008) *Mater Sci Eng A* 493:53
31. Jang S, Purohit Y, Irving DL, Padgett C, Brenner D, Scattergood RO (2008) *Acta Mater* 56:4750